JOURNAL OF SPACECRAFT AND ROCKETS
Vol. 33, No. 3, May–June 1996

Data Analysis and Model Comparison for Solar Array Module Plasma Interactions Experiment

Carmen Perez de la Cruz* and Daniel E. Hastings†
Massachusetts Institute of Technology, Cambridge, Massachusetts 02139
and
Dale Ferguson‡ and Barry Hillard§
NASA Lewis Research Center, Cleveland, Ohio 44135

Analysis of the Solar Array Module Plasma Interactions Experiment flight data from STS-62 was conducted to examine the relationships between the arc rate and the various solar-cell properties, environmental variables, and solar-cell parameters. The data indicate the existence of a critical ion flux, a critical neutral density, a threshold voltage for arcing to occur, and scaling of the arc rate with work function.

Nomenclature

A = Fowler–Nordheim coefficient, $1.54 \times 10^{-6} \times 10^{4.52\phi_w^{-1/2}}/\phi_w$ A/V^2
B = Fowler–Nordheim coefficient, $6.53 \times 10^9 \phi_w^{1.5}$ V/m
C_{diele} = capacitance of dielectric, F/m^2
C_{front} = capacitance of cover-glass front surface, F
d = thickness of dielectric, $d_1 + d_2$, m
d_1 = thickness of cover glass, m
d_2 = thickness of adhesive, m
d_{gap} = gap distance between cathode and anode, m
d_i = distance of electron first impact point from triple junction, m
E_e = electric field at emission site, V/m
E_i = electron incident energy on dielectric plate, eV
$E_{\max}$ = electron incident energy for maximum secondary-electron yield, eV
E_{TJ} = electric field at triple junction, V/m
m_e = electron mass, kg
m_i = ion mass, kg
n_e = plasma number density, m^{-3}
R = arc rate, s^{-1}
S_{FN} = emission-site area determined from Fowler–Nordheim plot, m^2
S_{real} = emission-site area determined by allowing for electron space-charge effects, m^2
T_i = ion temperature, eV
V_{arc} = voltage at which last arc occurred, V
V_b = bias voltage of interconnector (conductor), V
V_e = voltage that minimizes arcing time, V
V_i = initial voltage before solar-cell charging, V
v_{ion} = mean speed of ions entering sheath, m/s
y = distance of emission site from the triple junction, m
β = field enhancement factor
ΔQ = charge lost from one cover glass by one discharge, C
ϵ_{d1} = relative dielectric constant of cover glass
ϵ_{d2} = relative dielectric constant of adhesive
ϕ_w = work function, eV
γ_{ee} = secondary-electron yield
$\gamma_{\max}$ = maximum secondary-electron yield at normal incidence
η = factor allowing for difference in electric field at emission site and triple junction
τ_{arc} = time between arcs, s
τ_{efee} = enhanced-field electron emission charging time, s
τ_{ion} = ion charging time, s
τ_{exp} = experiment time, s
ξ = factor allowing for difference of dielectric constants between cover glass and adhesive

Received July 6, 1995; revision received Feb. 22, 1996; accepted for publication Feb. 22, 1996.

*Research Assistant, Department of Aeronautics and Astronautics.
†Professor of Aeronautics and Astronautics, Department of Aeronautics and Astronautics. Associate Fellow AIAA.
‡Branch Chief, Space Environment Interactions Branch. Member AIAA.
§Engineer, Space Environment Interactions Branch. Member AIAA.

Introduction

HIGH-VOLTAGE solar arrays have been observed to interact with the plasma environment of low Earth orbit (LEO) in two distinct manners. For positive voltage biases the current collection can be anomalously large, possibly leading to surface damage. For negative biases below a voltage threshold, approximately −200 V, arc discharges can occur. Experimentally, an arc discharge on a solar cell has been defined as a sudden current pulse up to the order of one ampere and lasting a few microseconds or less. Arcing can cause electromagnetic interference with instruments and damage to the solar cells.[1] Thus, there is a design tradeoff between high voltages and damage from arcing unless solar cells can be designed to mitigate or even eliminate arcing.

Conventional cells have the metallic interconnector between cells exposed to space. These cells arc both on the interconnector and on the cell edges.[2]

To eliminate the interaction between the conducting surfaces and the ambient plasma, these surfaces may be covered with an insulator. This isolation of conducting surfaces from the space plasma is the principle behind the design of a new type of solar cell, the wrapthrough-contact (WTC) solar cell, developed by NASA for the Space Station (SS).[3] The interconnectors of these cells are no longer exposed to the plasma, but instead pass underneath the substrate and connect to the middle of adjacent cells under the cover glasses. However, in this new design, the semiconductor is still exposed to space along the edge of the cell.

Arcing on high-voltage solar arrays has been observed in both ground and space experiments. The first observation of arcing on solar cells in a plasma chamber was made by Herron et al.[4] in 1971. The solar cells were biased between ±16 kV, and arcing was observed at bias voltages as low as −6 kV with a plasma density of 10^8 m^{-3}. The occurrence of arcs in space was verified by the first plasma interactive experiment (PIX I) in 1978. PIX I, flown as an auxiliary payload on Landsat 3's Delta rocket, obtained data for a period of 4 h in a 920-km polar orbit. During this period, a solar array consisting of twenty-four 2 × 2 cm conventional silicon solar cells was biased to ±1000 V. Arcing was observed at voltages greater than −750 V.

A more extensive experiment was conducted by PIX II in 1983. A more sophisticated version of PIX I, PIX II, was also flown as an auxiliary payload on a Delta launch vehicle into a 900-km polar orbit. In this experiment the solar array consisted of 500 conventional silicon cells, again biased to ±1000 V. Arcing was observed at voltages as low as −255 V. A few problems were encountered when interpreting the flight data. Unexpected tumbling of the spacecraft placed the Langmuir probe in the spacecraft wake, making its readings unreliable. Furthermore, if an arc occurred at high voltage, the power supply was often shut down for the rest of the data-taking cycle. The data from the PIX II flight and ground tests were studied by Ferguson,[5] who concluded that the arc rate $\dot{R}$ was directly proportional to the plasma density and varied as a power of the bias voltage.

The arcing onset mechanism proposed by Hastings et al.[6–8] modeled the arc initiation process at the triple junction, the point where the dielectric, conductor, and plasma meet.

In this paper we analyze the data from a recent flight experiment designed to study the interaction of high-voltage solar arrays with the plasma environment. In this experiment, different solar cells, space materials, and arc mitigation strategies were tested. This experiment was the Solar Array Module Plasma Interactions Experiment (SAMPIE).

SAMPIE Description

The SAMPIE was designed to study the arcing behavior and current collection characteristics of different solar cells and materials likely to be exposed to the LEO environment in future missions. Solar Array Module PIX was developed at the NASA Lewis Research Center and sponsored by the NASA Office of Aeronautics and Space Technology. The flight experiment was flown onboard the Space Shuttle Columbia in the STS-62 mission launched on March 4, 1994. The Orbiter was placed in a nearly circular orbit with 38.92-deg inclination and 300-km altitude.

Diagnostic Instruments

The Hitchhiker-M carrier for the Shuttle payload bay was configured for the OAST-2 mission, with the SAMPIE package on one of the four top mounting positions. The plate containing the cells to be biased was mounted on top of the metal box, whereas most of the instruments and electrical subsystems were placed inside the box. A pressure gauge was also included to measure the background pressure. The gauge could measure ambient pressures from 10^{-7} to 10^{-3} torr. Two high-voltage power supplies (HVPS-1 and HVPS-2) in the electronics box biased the specified cells to predetermined dc voltages, ranging from +300 to −600 V, above that of the orbiter. In addition, an electrometer in the HVPS-1 circuit measured the currents collected, and a sun sensor located on the experiment plate confirmed the attitude of the orbiter. Two additional electrical probes were also part of the package: a Langmuir probe to monitor the plasma density and temperature, and a V-body probe to monitor the shuttle's potential with respect to the plasma. It was estimated that SAMPIE would disturb the ionosphere within 1 m in all directions,[9] and consequently these probes were positioned about 5 ft away from the box.

Individual Experiments

A layout of the experiment plate is shown in Fig. 1. In the experiments, different technologies and arcing mitigation strategies were tested. A detailed description of all the experiments is given in Ref. 10. Among the cells tested was a coupon of four 8 × 8 cm WTC cells to be used on the International SS Alpha, a coupon of twelve 2 × 4 cm thin advanced photovoltaic solar array (APSA) cells, and a coupon of four traditional 2 × 2 cm silicon solar cells used to provide a baseline for comparison.

The SS cells were designed to operate in LEO at a nominal voltage of −160 V. The cells are mounted on a flexible substrate, and the intercell connections are made through copper traces imbedded in the substrate and welded to the back of the solar cells. The cover glass, semiconductor, and substrate of these cells were each 203 μm (8 mils) thick, and there was only about a 0.81-mm separation between adjacent cells. The semiconductor is silicon, the substrate is Kapton®, and the cover glass is ceria-doped microsheet (CMX).

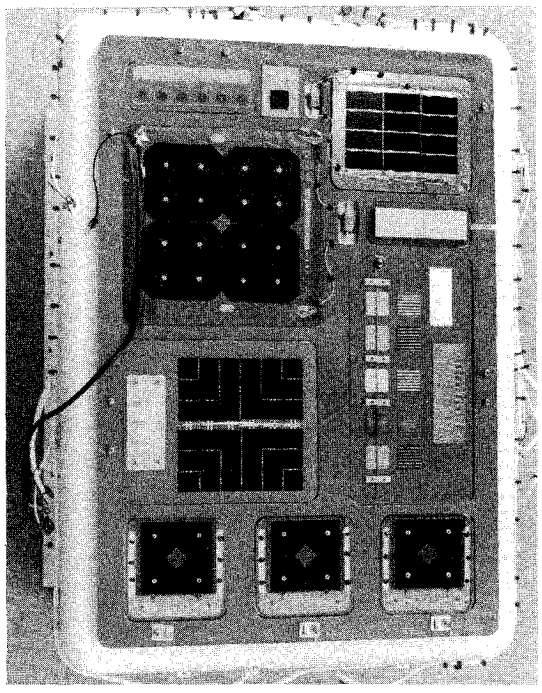

Fig. 1 SAMPIE plate.

The APSA cells, built by TRW, presented a thinner silicon-cell design. Their reduced thickness, 63.5 μm (2.5 mils), is expected to yield mass savings in future space applications. The thicknesses of the CMX coverglass and the Dow Corning adhesive DC-93500 are 51 μm (2 mils) and 76 μm (3 mils), respectively. The interconnector between these cells is silver-plated invar.

Lastly, the conventional silicon cell, representative of the cell technology presently used in many U.S. Department of Defense, NASA, and commercial spacecraft, was also tested. These cells were manufactured by Spectrolab Inc. and incorporated into an array by RCA in 1984. The thickness of the fused silica cover glass and the DC-93500 adhesive are 153 and 37 μm, respectively. The interconnector between these cells is assumed to be Kovar®.

To test different arcing mitigation strategies, three coupons of modified SS cells were tested. The size of these cells was reduced from the standard 8 × 8 cm to 3.5 × 3.5 cm. In each of the coupons, a different arc mitigation strategy was tested. In the first set (SSMIN-3), the side of the cover glass overhangs the cell by 0, 101.6, 177.8, and 279.4 μm (0, 4, 7, and 11 mils). In the second set (SSMIN-2), all four cells were shorted together. The excess adhesive was removed from the edges of the cells using a proprietary process developed by Physical Sciences Incorporated (PSI). In the third coupon (SSMIN-1), the cells had their edges completely covered with the cover-glass adhesive except for specified lengths, 0, 203.2, 406.4, and 812.8 μm (0, 8, 16, and 32 mils), which were exposed to the plasma.

On the right-hand side of the experiment plate, there are five metal samples, each made of a different pure metal: gold, silver, copper, aluminum, and tungsten. On top of these 1-in.-square samples are eight Kapton strips placed 0.0625 in. apart. A picture of the metal coupons in shown in Fig. 2. To provide a control, a second set of metal samples with a 1-mm-diam rod suspended 1 mm above the metal's surface was also tested. The distance above the metal was chosen to obtain an average electric field close to the samples of the first set, thus eliminating the dielectrics from the process. The second set of tests isolate the metal's effect on the arcing process, whereas the geometry of the first set resembles the geometries found in solar cells. This metal–insulator geometry can be found in the triple junction of the conventional cells. The geometry of the Hastings–Cho arcing model[7] closely resembles that of these samples.

SAMPIE Operations

A low-voltage biasing sequence and different dwell times at each voltage were used in the arcing experiments. Two different

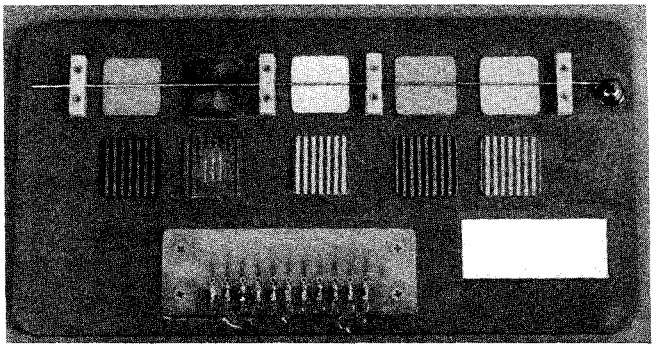

Fig. 2 Metal-coupon geometry.

high-voltage biasing sequences were used. The cells assigned to the HVPS-1 were biased to a maximum voltage of −600 V, and those in the HVPS-2 to −500 V. The metal samples and the modified SS cells treated by PSI were assigned to HVPS-2, and the rest of the cells in the arcing experiments were assigned HVPS-1. Arcs were detected by counting the number of spikes in the current flowing through the solar-array circuit above a threshold value. The threshold currents were set to 100 and 20 mA for the HVPS-1 and HVPS-2, respectively.

Each power supply biased a sample to a bias voltage given by the biasing sequence chosen. When the high-voltage sequences were executed, only one cell was biased at a time. The remaining samples were held at the ground potential.

Predictions and Data Comparison

SAMPIE Data Acquisition

During the experiment, preliminary data were received by the OAST-2 payload control center at the Goddard Space Flight Center. After 37 h of scheduled data taking, an anomaly with the HVPS-1 circuit necessitated reconsideration of the experiment timeline, and new instructions were transmitted to SAMPIE on orbit. A total of 62 h of current-collection and arcing data were obtained, stored on board, and recovered after Columbia returned to Earth. A total of 18 h and 46 min of arcing data were obtained in the bay-to-ram orientation, and 24 h of data were obtained in the bay-to-deep-space orientation.

During the experiment, the neutral pressure and orbiter potential were continuously monitored. The V-body probe showed that the potential of the Shuttle never differed from that of the ambient plasma by more than ±3 V during the arcing experiments. Therefore, the potentials of the cells with respect to the plasma environment are accurately represented by the applied bias voltages.

Approximately every 3 min, the Langmuir probe performed a plasma density and temperature sweep. Standard probe theory was used to obtain these parameters from the raw sweeps. However, these standard techniques did not yield the correct plasma parameters expected from a moderate-sized probe in a flowing plasma facing the ram direction. Both the plasma densities and the temperatures were uniformly higher than expected. The reason for this is unknown. However, in view of the uniformly higher results produced by the onboard instrumentation, it was necessary to correct the results. This was done by comparing the onboard data with ionosonde data taken as the Shuttle passed over several ionosonde stations.

A comparison between ionosonde data during times and locations coincident with the Shuttle orbit during the bay-to-ram data-taking period and the International Reference Ionosphere (IRI-86) model showed that the IRI model predictions are extremely good, especially in the daytime. Based on the IRI model, simple correction factors could be applied to the standard probe-theory results to yield accurate densities and temperatures. The corrections were the following: for plasma density, divide the experimental plasma densities by a factor of 3.6. The simulations and data analysis of the arc rate in the SAMPIE used the ambient plasma conditions obtained using these corrections. It is believed that the plasma densities are correct to within about 10% and the electron temperatures to within 0.03 eV.

The corrected plasma densities during a portion of the flight in the bay-to-ram orientation are shown in Fig. 3. The plasma density

Table 1 SAMPIE cell data

Cell type	Si	Si WTC	APSA	Gold sample
Manufacturer	RCA	NASA	TRW	—
Cell size, cm^2	2 × 4	8 × 8	2.6 × 5.1	0.158 × 2.54
No. of cells	4	4	12	8
Cell gap, μm	500	1000	635	1588
d_{cell}, μm	203	203	56	—
d_1, μm	153	203	51	25
d_2, μm	37	N/A	76	20
ϵ_{d1}	3.5	4	4	3
ϵ_{d2}	2.7	3	2.7	3.8
$\gamma_{max\,1}$	3.46	4	4	2.1
$\gamma_{max\,2}$	3	2	3	—
$E_{max\,1}$, eV	330	400	400	150
$E_{max\,2}$, eV	300	200	300	—
ϕ_w, eV	4.76	4.85	4.26	5.1

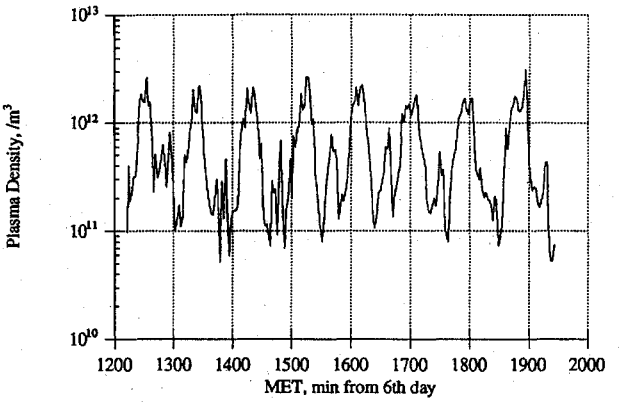

Fig. 3 Plasma density measured by SAMPIE (corrected) in ram.

shows peaks and valleys about every 90 min, the period of the orbit. The peaks correspond to when the shuttle receives sunlight and therefore measures the daytime plasma environments, and the valleys correspond to when the shuttle is in eclipse and the nighttime plasma parameters are measured. No corrected values of the Langmuir-probe data were available for the bay-to-deep-space orientation period. The plasma density used in that period for the simulations was inferred from the IRI-86 model.

The cell temperatures annotated during the preliminary telemetering to the payload control center are also included. Some data points were excluded for various reasons, such as anomalously high arc counts or the concurrent operation of other experiments in the Shuttle bay. In the bay-to-space data, an increase in arc rate and neutral pressure was observed when gas was released during the experimental investigation of shuttle glow experiment. Arc counts above 1000 were considered anomalously high. When the anomaly in the HVPS-1 circuit occurred, the number of arcs detected increased from tens of arcs to counts ranging from 1000 to 3000. Therefore, arc counts above 1000 were discarded. Because of the anomaly in the HVPS-1, the arcing data obtained from the silicon, APSA, and WTC cells are limited to a few experiments in the bay-to-ram orientation. The metal coupons, however, were additionally biased in the bay-to-deep-space orientation, providing valuable data.

SAMPIE Simulations

The predictive capability of the modified semianalytical code described in the papers by Cho and Hastings[7,8] was verified by generating arc rates for the conventional cells and metal samples biased during the flight experiment. These arc rates were based on the experimental data obtained from the flight experiment and were then compared with the experimental rates. The given and assumed properties for the conventional, the WTC, and a selected metal coupon are summarized in Table 1. The geometry of the five metal coupons with the Kapton strips closely resembles that of the proposed model. The only property differing between the metal samples is the work function of the conductor. The work function ϕ_w is a measure of the ease with which electrons are released from the surface. The

Table 2 Work functions of the metal samples and oxides

Metal	ϕ_w, eV Pure metal	Oxide
Gold	5.1	——
Copper	4.65	5.02
Tungsten	4.55	4.95
Aluminum	4.28	4.7
Silver	4.26	4.68

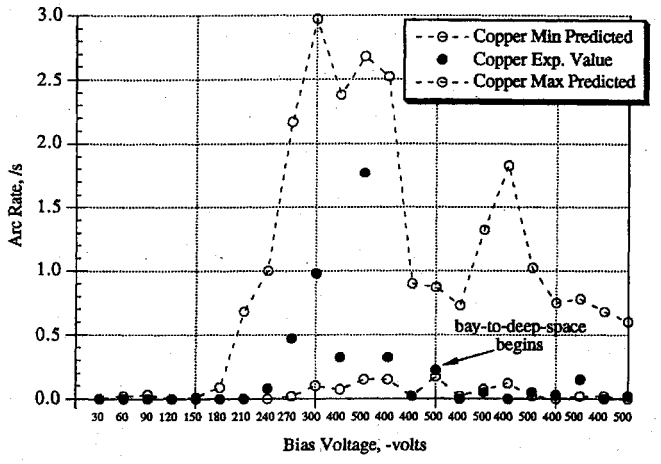

Fig. 4 Experimental and simulated arc rates for the copper coupon.

given and assumed work functions for the metals and their oxides are shown in Table 2 (Refs. 11 and 12).

Whenever possible, the environmental data measured by SAMPIE were used in the simulations. Since the cell temperature was not annotated for all the experiments, the range used was that observed during the bay-to-ram portion of the experiment, −5 to 15°C. These temperatures provided a maximum and a minimum arc-rate value for each run. Values for those environmental variables not recorded during the flight experiment, such as ambient neutral temperature, ion mass, and ion velocity in the ram orientation, were generated using the Environmental Work Bench (EWB) package. The variation of these parameters during an orbit was small, and therefore average values for these variables were used. The simulations also included the experimental current threshold: 100 mA for the silicon and APSA cells and 20 mA for the metal coupons.

The dynamic range in plasma density and neutral density for the cells and the metal coupons is very small. However, the range in the ion velocity is large for the metal coupons. This is because the coupons were biased in the bay-to-deep-space orientation, where the ions no longer arrive at the front surface with orbital velocity, but with the thermal velocity. A comparison between the arc rates obtained by the simulations and the experimental values for the silicon and APSA cells was made. In general, the experimental values fall between the maximum and minimum simulated arc rates. For the silicon cell at −600 V, the semianalytical code underpredicts the arcing rates, but the simulated values are of the same order of magnitude as the experimental values. A trend is seen in both the experimental and simulated data: the arcing activity greatly decreases when the Shuttle is in the bay-to-deep-space orientation.

Similar comparisons were generated for each of the metal samples. A typical example is shown in Fig. 4. The model accurately simulated the arcing activity of the copper coupon and the tungsten coupon, but underpredicted that for the gold sample at the high voltages. It is interesting to note how the maximum predicted arc rates show the same trends seen in the actual data. In the next section, the dependence of the arc rate on various parameters such as the work function will be examined using the flight data from these metal samples.

Data Analysis of SAMPIE Data

In this section, the dependence of the arc rate on several variables suggested by the semianalytical model will be discussed. These dependences will be then examined in the arcing data obtained from the SAMPIE experiment.

Parameters Influencing Arcing

From the model proposed by Hastings et al.,[6–8] it is possible to identify operational parameters, environmental variables, and material and geometric properties that will affect the arc rate. The arcing onset mechanism is described by the following sequence:

1) Ambient ions, attracted by the negatively biased conductor, charge the dielectric front surface (parallel to the conductor), but leave the side surface effectively uncharged.

2) As the potential of the front surface approaches zero, a strong electric field, given by $E = V_b/d$ (where V_b is the bias voltage and d the dielectric thickness), is set up between the triple junction and the front surface.

3) This strong electric field, aided by field enhancement at sites in the conductor surface, induces a prebreakdown enhanced-field electron emission (EFEE) current showing the characteristic of the Fowler–Nordheim emission current. In addition, electrons are released on account of the bombardment of the conductor surface by the ambient ions.

4) Some of the emitted electrons strike the side surface of the dielectric, causing the release of secondary electrons and the electron-stimulated desorption of neutrals adsorbed on the dielectric surface. If the secondary-electron yield is greater than unity and the electrons have an escape path, the side surface charges up positively, providing a positive feedback mechanism to further enhance the electric field at the conductor surface.

5) As the electric field increases, the electron emission current increases until it is limited by the negative space charge of the emitted electrons.

6) Once the neutral density becomes high enough, ionization begins due to collisions between electrons and neutrals.

7) Even if the density is not high enough for Townsend breakdown to occur, breakdown is still possible if the positive ion space charge can cancel the negative electron space charge and enhance the field at the conductor.

8) The arcing time is the minimum of the sum of the ion and EFEE charging times for all the emission sites on the conductor.

9) A discharge wave created by the arc resets the charging process at all of the emission sites within the area covered by the wave.

The dependence of the arc rate on the bias voltage, electron work function of the interconnector material, dielectric thickness, front surface area, overhang of the cover glass, ion flux, neutral flux, and cell temperature will be examined. In general, the arc rate can be expressed as function of these quantities and is the reciprocal of the time between arcs.

When an arc occurs, the cover glass is recharged by ions and the electric field at the triple junction increases. The EFEE process may start whenever the surface of the conductor feels a strong enough electric field. The total charging time for each emission site is determined numerically by finding the value of V_e that minimizes

$$\tau_{\text{chrg}} = \frac{\{V_e - [V_{\text{arc}} - (\Delta Q/C_{\text{front}})]\}C_{\text{front}}}{en_e v_{\text{ion}} A_{\text{cell}}} + \frac{C_{\text{diele}} d_i^2}{(\gamma_{ee} - 1)\sqrt{S_{\text{real}}}\eta\xi A(S_{\text{FN}}/S_{\text{real}})B\beta} \exp\left(\frac{Bd}{\beta\eta\xi_0 V_e}\right) \quad (1)$$

This expression assumes that the time during which the neutrals are ionized is short and therefore can be neglected.

Bias Voltage

The dependence of the arc rate on the bias voltage is obtained by setting the remaining parameters equal to constants. Equation (1) suggests the following functional form:

$$\dot{R} = \frac{1}{c_0 \exp(c_1/V_b) + c_2 V_b} \quad (2)$$

At low voltages, the electric field at the triple junction will be small and the charging time will be dominated by the EFEE term. Thus, the ion charging time may be neglected. Since the EFEE

charging time decreases exponentially with increasing V_b, the arc rate will increase exponentially with V_b. This exponential dependence gives an effective threshold voltage: the voltage at which the EFEE charging time is on the order of the experiment time. No arcs have been observed above −96 V, the operational voltage used in European spacecraft; therefore, the threshold voltage is above this value. The threshold voltage is close to −100 V when the experiment time is on the order of 100 s.

Material Properties and Cell Area

Under normal conditions, electrons are prevented from leaving a metal by a potential step at the interface. The height of this step is the work function. If given sufficient energy, the electrons will escape. Metals with higher work functions will exhibit lower electron emission from the conductor's surface. Thus, the time needed for the electric field to run away will be increased with increasing work function. The work function is included in the Fowler–Nordheim coefficients in the τ_{efee} equation. With the arc rate defined as $1/\tau_{\text{chrg}}$ and the other parameters held constant, the dependence of the arc rate $\dot{R}$ on the work function ϕ_w is given by

$$\dot{R} = \frac{1}{c_0\sqrt{\phi_w}\,10^{4.52/\phi_w}\exp\left(\phi_w^{1.5}\right) + c_1} \tag{3}$$

The dependence on the work function is more pronounced for low bias voltages, where the τ_{ion} term, c_1, may be neglected. The presence of the work function in the exponential ensures that the arcing activity will be greater for interconnectors with lower work functions.

The area of the front surface of the cell will also affect the arcing rate. The model suggests that the arc rate will vary linearly with the number of correlated areas encompassed by the cell. Therefore, the arc rate will be affected by an increase or decrease in the number of correlated areas. Although the cell area is present in the τ_{ion} expression, its effect is canceled by the cell-area factor in the capacitance of the dielectric front surface.

Environmental Variables

The semianalytical model predicts that there is a critical ambient ion flux. If the ion flux is below this value, the electric field created by the ions deposited on the front surface will not be sufficient to start the EFEE from the conductor surface. In this case, the ion charging time τ_{ion} will be greater than the experiment time τ_{exp}. Thus, no arcs will occur during the experiment. The critical ion flux, $\Gamma_{i\,\text{crit}}$, calculated by setting τ_{ion} equal to τ_{exp}, is given by

$$\Gamma_{i\text{crit}} = \frac{\Delta V_{\text{drop}}\, C_{\text{front}}}{e A_{\text{cell}}\, \tau_{\text{exp}}} \tag{4}$$

where ΔV_{drop} is the voltage drop during an arc. For given dielectric constants, the critical ion flux will vary linearly with this drop. If the voltage drop varies with the bias voltage, then so will the critical ion flux. If τ_{ion} is less than τ_{exp}, a further dependence can be derived from Eq. (1). Keeping the remaining parameters constant, the arc rate $\dot{R}$ is given by $\dot{R} = 1/(c_0/\Gamma_i + c_1)$. At very large voltages, where the EFEE term can be neglected, the expression suggests that the arc rate varies linearly with ion flux.

The cell temperature and neutral flux onto the side surface determine whether the desorbed neutral density is sufficient to allow breakdown to occur. For a given cell temperature, there is a critical neutral flux below which breakdown will not occur. If the ambient neutral flux is below this value, the surface cannot be recharged during the experiment time. Lower cell temperatures result in a larger number of neutrals on the surface available, and consequently a lower ambient neutral flux is needed for breakdown to occur. Similarly, for a given neutral flux and experiment time, there is a cell temperature above which not enough neutrals will reside on the surface to allow breakdown. If the arc rates are measured while the cells are always at the same angle of attack, the neutral flux will vary with neutral density and with the temperature of the neutrals. The cells in the SAMPIE were oriented in the ram and in the bay-to-deep-space orientations. In the ram orientation the flux to the side surface of the solar cell is only due to neutrals moving with thermal velocities. Since the experiment was placed in the Shuttle bay, it will be assumed that the side surface of the cells while in the latter orientation was also charged only by the thermal flux. Therefore, these orientations become indistinguishable with respect to the neutral flux. If the temperature of the neutrals is assumed to be constant, the neutral density and flux become interchangeable parameters in the data analysis.

Data Analysis of Conventional Silicon Cells and APSA Cells

Because of the anomaly in the HVPS-1 circuit, only one low-voltage bias sequence and two high-voltage biasing sequences were executed for the silicon cells. For the APSA cells there was only one data set taken. The arcing rates are zero at bias voltages below and including −400 V, and they show a sharp increase at the high voltages. The limited data preclude a determination of the threshold voltage, but support the conclusion that for bias voltages above −400 V, the silicon and APSA cells will arc. Because of the scarcity of data points, no correlations were found between the arc rate and the other parameters. Consequently, the arcing data from these cells were used to make qualitative comparisons with other cells.

Data Analysis of Metal Coupons

The number of data points for the metal coupons was large compared to that for the other cells. One arcing measurement is available at each voltage of the low-voltage bias sequence. For each of the metal samples biased at high voltages (−400 and −500 V), two data points were obtained when the cells were oriented in the ram direction, and five data points in the bay-to-deep-space orientation. This large number of data points allowed relationships between the arc rates and the different environmental variables and operational parameters to be examined. It is expected that the data from these coupons will agree very well with the model predictions because of the close resemblance of the geometry of the coupons to the geometry assumed by the model. The only difference between the different coupons is the work function of the metal, which represents the interconnector in the model. As suggested by the model, the dependence of the arc rate on the following experimental parameters was examined:

Parameter	Minimum	Maximum
Bias voltage, V	−30	−500
Work function, eV	4.26	5.1
Ion flux, $m^{-2}\ s^{-1}$	1.6×10^{14}	2.6×10^{16}
Neutral density, m^{-3}	3.7×10^{15}	2.4×10^{16}
Cell temperature, K	268.1	288.1

To examine the correlation between the arc rate and a given parameter, points along the orbit were found where the remaining parameters were constant (using 5% tolerance for the voltages and 15% for the other quantities). A plot of arc rate vs the parameter was then generated. The data points showing anomalous high arc rates, caused by the failure in the HVPS-1 circuit or the concurrent operation of other experiments in the Shuttle bay, were ignored.

Dependence of Arc Rate on Cell Temperature

The dependence of the arc rate on the cell temperature could not be determined, owing to the small number of data points as well as to the limited dynamic range of this parameter, 268–288 K.

Dependence of Arc Rate on Neutral Density and Ion Flux

When the effect of the ion flux or the neutral density was studied, the other environmental parameters were not held constant, because the data showed two distinct populations: high values of ion flux and neutral density when in ram, and low values when in the bay-to-deep-space orientation. These distinct populations are shown in Fig. 5. If one of these two parameters was held constant to study the other, then only one of these populations would show, and no correlations could be determined.

The neutral flux cannot be determined from the experimental data, but the neutral density may be calculated from the neutral pressure if a neutral temperature is assumed. An average neutral temperature

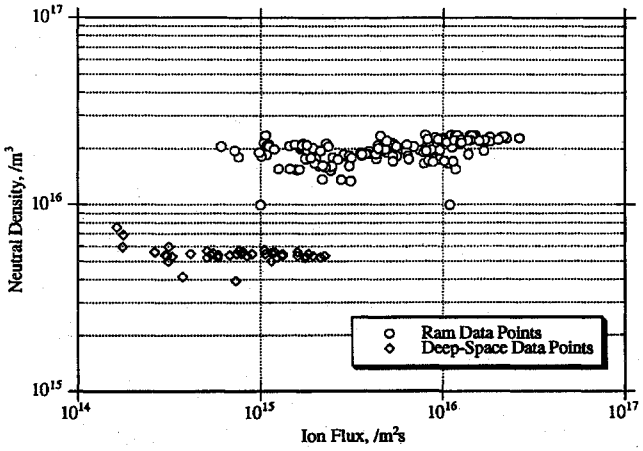

Fig. 5 Neutral density and ion flux for SAMPIE arcing data for all voltages.

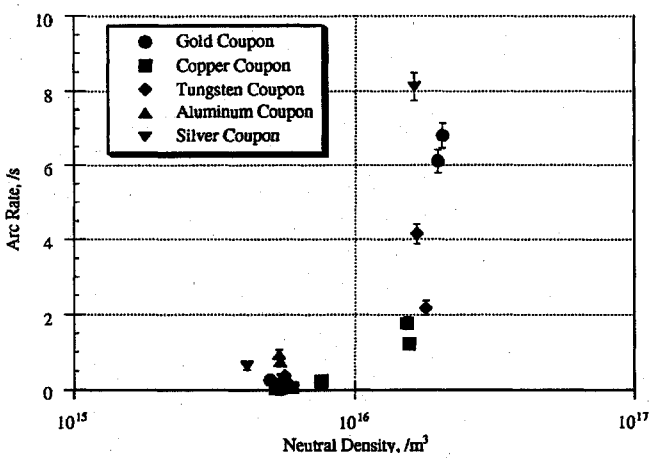

Fig. 6 Arc-rate dependence on neutral density at −500 V over all ion fluxes.

of 1100 K obtained from the MSIS-86 model was used. The neutral densities calculated from the experimental neutral-pressure measurements yielded values about two orders of magnitude larger than the ambient density given by MSIS-86. This increase in the density surrounding the Shuttle has been observed during many Shuttle experiments and is attributed to nearby thruster firings.

The behavior of the arc rate with respect to neutral density is shown in Fig. 6. The data suggest that there is a neutral density above which the arcing activity increases dramatically, about 5×10^{15} m^{-3}. It is expected from the model that for a given cell temperature and voltage, there will be a critical ambient neutral density above which arcing will always occur once the EFEE emission has started. These data support the existence of such a threshold.

The dependence of the arc rate on the ion flux for all the metal coupons at −400 V is shown in Fig. 7. As expected from the model, the plot seems to show a critical ion flux above which arcing always occurs. The figure shows a critical ion flux of about 5×10^{14} m^{-2} s^{-1}. The critical flux calculated using Eq. (4), assuming a ΔV_{drop} of 300 V, was about 2×10^{13} m^{-2} s^{-1}. To obtain the critical ion flux shown in the data, the average voltage drop would have to be 1500 V, which is impossible. The range in the bias voltage was not large enough to test the linear dependence of the critical flux on the bias voltage, as hypothesized by the model.

In summary, the experimental data support the existence of a critical neutral density and ion flux as predicted from the model. The two distinctive populations shown in Fig. 5 preclude the study of the arc-rate behavior with respect to only one of these parameters. Therefore, the dependence of the critical ion flux on the bias voltage or the agreement of the data with the breakdown criterion predicted by the model could not be determined. Yet, the experimental data do show that as both the ion flux and the neutral density increase, the arc rate increases.

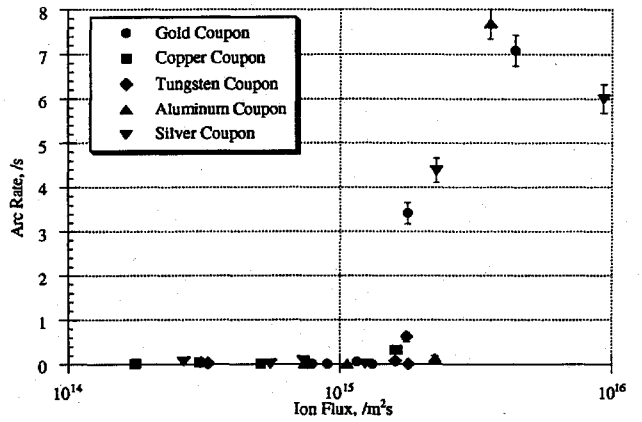

Fig. 7 Arc-rate dependence on ion flux at −400 V over all neutral densities.

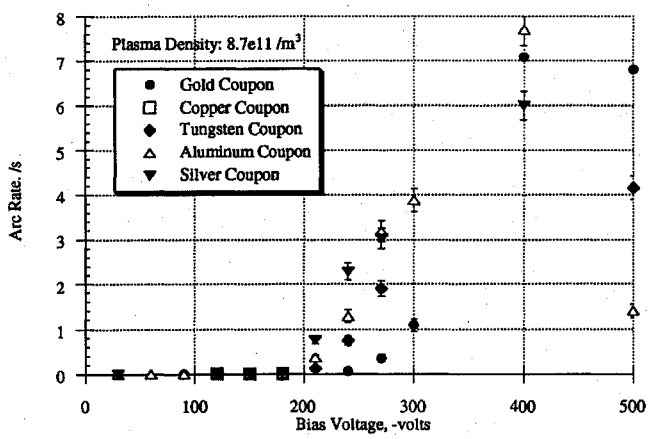

Fig. 8 Arc rate at points of constant plasma density: neutral density $\approx 2 \times 10^{16}$ m^{-3} and cell temperature ≈268–288 K.

Dependence of Arc Rate on Bias Voltage

The dependence on the bias voltage while keeping plasma density constant was examined in the ram data, where the bias voltage ranged from −30 to −500 V. There is a clear correlation between arc rate and bias voltage, shown in Fig. 8. At the low voltages no arcing occurs, and beyond the threshold voltage, between −180 and −210 V, the arc rate increases dramatically.

The data analysis focused on the determination of the dependence of the arc rate on this parameter. Because the work functions of pure silver and aluminum differ by only 0.02 eV, the data for these coupons were combined to increase the number of data points and consequently the statistical significance.

The data were fitted using an exponential form and the Cho–Hastings model form as given by Eq. (2). The fits were done using a least-squares fit to a nonlinear equation using the gradient expansion method. Data points indicating anomalous arc counts (above 1000) were not included in the data fitting. A very low arc count of 84 for the aluminum sample at −500 V was also discarded. When this data point was included, the Cho–Hastings model fit did not converge.

The exponential fit is derived from the simple form of the Cho–Hastings model as given by Eq. (2). When the bias voltage is low, the exponential term will dominate, and the equation can then be rewritten as

$$\dot{R} = \frac{1}{c_0 \exp(c_1 / V_b)} \tag{5}$$

For the metal coupons, the coefficients c_0 and c_1 vary only with the work function, since they include the Fowler–Nordheim coefficients. The exponential fit to the silver–aluminum coupon data at lower voltages, shown in Fig. 9, yields the following equation:

$$\dot{R} = \frac{1}{0.005 \exp(1152 / V_b)} \qquad \text{(silver–aluminum)} \tag{6}$$

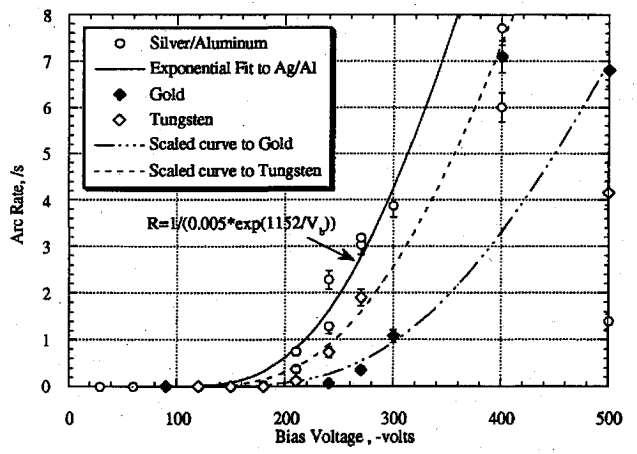

Fig. 9 Exponential fit to Ag–Al combination and scaled curves for Au and W: ion flux $\approx 6.4 \times 10^{15}$ m^{-2} s^{-1}, neutral density $\approx 2 \times 10^{16}$ m^{-3}, and cell temperature $\approx$268–288 K.

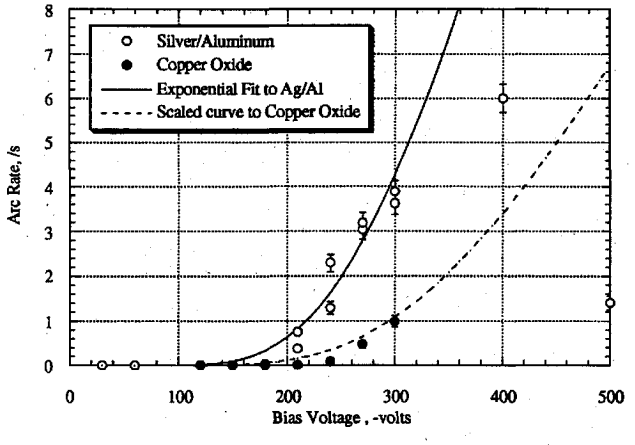

Fig. 10 Exponential fit to Ag–Al combination and scaled curves for oxidized Cu: ion flux $\approx 1.6 \times 10^{16}$ m^{-2} s^{-1}, neutral density $\approx 2 \times 10^{16}$ m^{-3}, and cell temperature $\approx$268–288 K.

This exponential form provides a good fit, but if the average values of parameters such as β and S_{FN} are substituted in the τ_{efee} expression, the resulting coefficients c_0 and c_1 do not match those obtained from the fit. The coefficients c_0 and c_1 from the exponential fit for a given work function ϕ_w, scaled for a different work function ϕ_{w2}, yield the new coefficients, c_{02} and c_{12}, given by

$$c_{12} = \left(\frac{\phi_{w2}}{\phi_w}\right)^{1.5} c_1 \tag{7}$$

$$c_{02} = 10^{-4.52(1/\sqrt{\phi_w})-(1/\sqrt{\phi_{w2}})} (\phi_{w2}/\phi_w)^{\frac{1}{2}} c_0 \tag{8}$$

If the coefficients from the exponential fit to the silver–aluminum combination are accordingly scaled for the work function of gold, $\phi_w = 5.1$ eV, and the work function of tungsten, $\phi_w = 4.55$ eV, the lower curves of Fig. 9 are obtained. Both curves seem to fit the data well. However, a photograph of the samples taken after the flight suggests that the silver sample and the copper sample were oxidized. The work functions of the oxides are shown in Table 2. Note that the work function of copper oxide is very close to that of gold, which may explain the nearly identical arc rates observed for these coupons. Since the arc rates of the silver and aluminum were very close, the work function of the aluminum sample was set equal to that of the silver oxide. Using the new work functions for the oxides, the scaled curves from the aluminum–silver exponential fit to the other samples no longer seem to fit the data well. If, on the other hand, the work function of the pure aluminum or silver is scaled with respect to that of the oxidized copper sample, the scaled curve, shown in Fig. 10, fits the copper data well, indicating that the copper oxidized. The scalings suggest that the silver and aluminum samples may not have oxidized completely. Another possible explanation is that the work function of the metal has been changed by the adsorption of

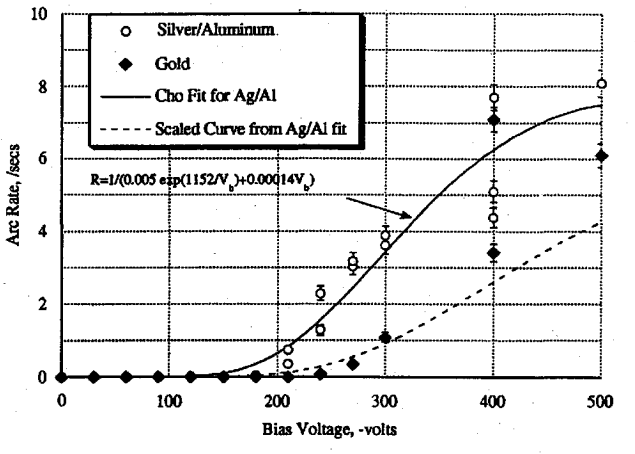

Fig. 11 Cho–Hastings simple fit to Ag–Al combination and scaled curve for Au: ion flux $\approx 6.4 \times 10^{15}$ m^{-2} s^{-1}, neutral density $\approx 2 \times 10^{16}$ m^{-3}, and cell temperature $\approx$268–288 K.

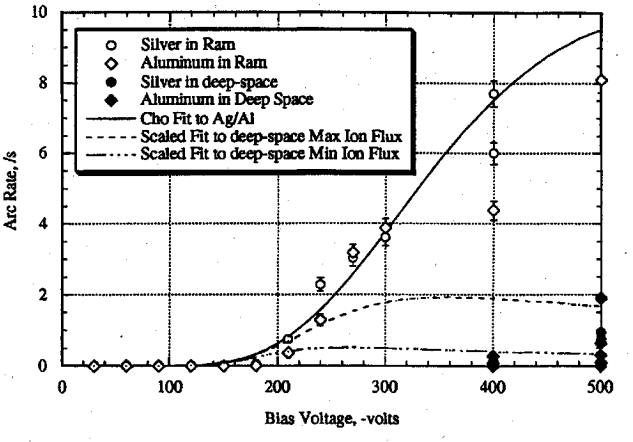

Fig. 12 Cho–Hastings simple fit to Ag–Al combination and scaled curve for ion fluxes: cell temperature $\approx$268–288 K.

gas on the surface.[13] The effect of the adsorbed gas was not included in the semianalytical model. The change in ϕ_w depends strongly on the binding state, and for the same combination of gas and solid, one adsorbing state gives an increase of ϕ_w, while others give a decrease. Therefore, it is possible that the aluminum sample did oxidize, but the adsorbed gas on its surface reduced its work function to a value close to that of pure aluminum.

The exponential form overpredicts the experimental values at the high voltages. Therefore, an additional term is needed in the denominator of Eq. (5) to lower the arc-rate values at the high voltages. The functional form suggested by Eq. (2) contains this additional term and was also used to fit the data. Using the values of the coefficients obtained in the exponential fit, a value for the coefficient of the τ_{ion} term was found. The resulting fit yielded the following equation and is shown in Fig. 11:

$$\dot{R} = \frac{1}{0.005\exp(1152/V) + 0.00014V_b} \qquad \text{(silver–aluminum)} \tag{9}$$

This functional form also provides a good fit to the data. Again, the τ_{ion} coefficient found cannot be supported physically. The fit and the curve obtained when the fit is scaled for the gold work function are shown in Fig. 11.

Although the coefficients are not physically supported, a further scaling with ion flux was made using this functional form. Equation (9) may be scaled to allow for the lower ion flux in the bay-to-deep-space orientation. The only term affected by the ion flux is τ_{ion}, which is inversely proportional to it. From the SAMPIE diagnostic data, the ion flux decreased by about two orders of magnitude. Equation (9) scaled to the maximum and minimum ion fluxes encountered in the bay-to-deep-space orientation is compared with the experimental data in Fig.12. The scaled curves predict the arcing activity at lower ion fluxes very well.

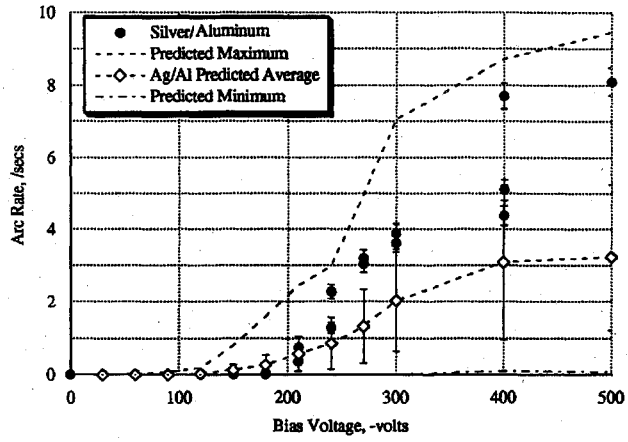

Fig. 13 Comparison of Ag–Al experimental data and numerical arc rates: $\beta = 200$, ion flux $\approx 6.4 \times 10^{15}$ m^{-2} s^{-1}, neutral density $\approx 2 \times 10^{16}$ m^{-3}, and cell temperature $\approx 268-288$ K.

Two different functional forms were used to fit the arcing data from the metal samples. The limited number of data points obtained at each voltage was not sufficient to determine the equation describing the relationship between arc rate and bias voltage. The functional forms provided equally good fits. Both the exponential and the Cho–Hastings model fit show an onset voltage at approximately −180 V, which seems to be supported by the data. The coefficients from these fits cannot be interpreted physically. Yet, as expected from the model, these coefficients scale with the work function at the lower voltages and with ion flux at the higher voltages. Since the coefficients cannot be supported physically, these coefficients cannot be used to predict the arcing activity of other cells. Yet, when the semianalytical code is used and parameters such as β and S_{FN} are chosen randomly from a distribution, the maximum and minimum arc-rate predictions bound the data very well.

The arcing code was used to predict the arcing activity of the silver–aluminum combination from Fig. 11. The code was run 100 times with an average β value of 200, and from these runs, the maximum, minimum, average, and standard deviations of the predicted arc rates were calculated. The results are shown in Fig. 13. At the higher voltages, the experimental data fall outside the one-standard-deviation error bars. At the lower voltages, below −240 V, the code predicts the arcing activity very accurately. The maximum and minimum expected arc rates bound all the experimental data.

Therefore, there are two possible ways to predict the arc rates for a given cell: to scale the coefficients from fits to this cell under a different ion flux or with a different interconnector material, or to use the semianalytical code. The former way is limited in that only data tabulated from flight experiments could be used, but in a given flight experiment data would need to be recorded only at a particular ion flux and the arcing activity at the other fluxes could be calculated from the observed behavior. The maximum and minimum predictions from the semianalytical code can predict the arcing activity of most cells under different environmental conditions.

Data Analysis of WTC Cells

As described previously, SAMPIE biased four different sets of WTC cells. The large SS cells are designated as SS. The set of modified cells completely sealed with adhesive except for specified lengths is designated by SSMIN1. SSMIN1,1 refers to the cell with no adhesive removed, and SSMIN1,4 refers to the cell with 32 mils removed, SSMIN3 refers to the set of modified cells in which the overhang length of the cover glass was varied. The cell with no overhang, used as a control, is designated by SSMIN3,1. The run number indicates the particular time during the experiment when a biasing sequence was executed, and the second number indicates the number of times the run was executed. In some cases, runs using the same sequence for the same cell are denoted by the same symbol. Low-voltage runs with zero arc rates at each bias voltage are shown with an open circle, and the high-voltage runs with an open square. Almost all of the cells showed no arcing at bias voltages lower than −300 V.

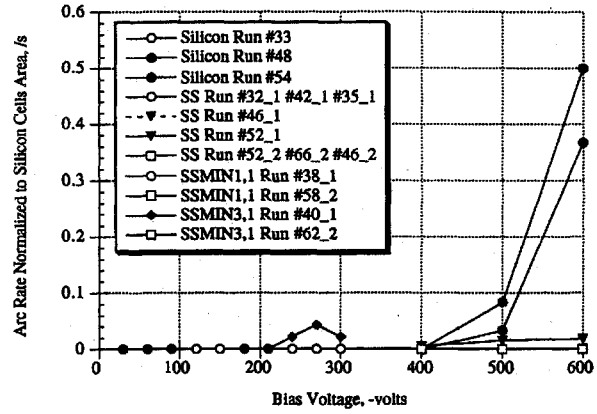

Fig. 14 Normalized arcing activity of silicon and SS cells.

The flight data obtained for the WTC cells were also limited, and therefore only qualitative comparisons could be made. For this reason, all the data were examined as if they were under similar environmental conditions. This assumption may induce some errors in the analysis. The WTC cells used as a control in the overhang study SSMIN3,1 arced at a surprisingly low voltage of −240 V. At the larger bias voltages, the experimental scatter is very wide. In one run (46), the SS cells arced very little at −600 V, but on another run (52), the arc count was as large as for the conventional cells (runs 48, 54). This large scatter suggests that the arcing problem may not be eliminated by shielding the interconnectors from the ambient plasma.

If the arc rates for each cell are normalized by the area, as suggested by the conventional geometry model, the arcing activity of the SS cells and silicon cells can be compared. Normalizing by the area of the silicon cells, Fig. 14 is obtained. The arcing activity exhibited by the SS cells is now much lower than that of the silicon cells, indicating that these cells may indeed have reduced arc rates.

Conclusions

The code based on the Hastings–Cho semianalytical model was used to simulate the arc rates in the silicon, APSA, and metal samples biased during the SAMPIE. The environmental parameters used in these simulations and the data analysis were those recorded during the experiment. The plasma density and electron temperature values obtained from the Langmuir probe during the ram portion of the experiment did not agree with the values expected from a moderate-sized probe in a flowing plasma. Both the plasma densities and temperatures were higher than expected. Therefore, correction factors for the ram orientation were calculated based on the agreement between the IRI-86 model and ionosonde measurements performed during the flight. These corrected plasma densities and temperatures were used for the predictions during the ram portion of the experiment. The values for these parameters in the bay-to-deep-space orientation were calculated using the IRI-86 model included in the EWB software package. In general, the predicted rates for the SAMPIE modeled accurately the arcing activity at the lower voltages, below −300 V, while it underpredicted the arcing for some of the metal samples at the higher voltages.

In the data analysis of the SAMPIE, correlations of the arc rate with material and geometric properties and with environmental and operational parameters were studied. These correlations helped to verify the validity of the semianalytical model. The limited data obtained for the silicon, APSA, and WTC cells allowed only qualitative comparisons to be made. The larger number of data points for the metal coupons allowed a quantitative analysis.

Arcing was observed in the standard silicon, APSA, and WTC cells and in the metal samples. Assuming that the arc rate varies linearly with the cell area, the arcing activity in the WTC cells was much lower than that of the silicon cells. Therefore, even though the WTC cell design has not completely suppressed arcing, it seems to have reduced it dramatically.

The dependences of the arc rate on the various parameters were studied in the metal-coupon data. No dependence on cell

temperature was supported by the data. This lack of a clear dependence is probably due to the limited range of cell temperatures. The dependence on the ion flux and neutral density could not be studied separately, because there were two distinct populations: high values of ion flux and neutral density while in ram, and low values while in the bay-to-deep-space orientation. The data support the existence of a critical neutral density and ion flux, and imply that as both these parameters increase, the arc rate also increases.

There is a clear dependence between the arc rate and the bias voltage. The arc rate is zero for the lower voltages, and at some voltage it increases sharply. The only difference between the metal coupons is in the work function of the interconnector material. The model predicts the arc rate will be lower for interconnectors with higher work functions and that this behavior will be more pronounced at the lower voltages where the enhanced-electric-field term dominates. This predicted behavior is supported by the flight data at voltages below −270 V.

The arc rate as a function of bias voltage was fitted using two different functional forms. The functional forms were derived from the model: at the lower voltages, the arc rate is expected to vary exponentially, and at the higher voltages, where the ion charging time may no longer be neglected, the data were fitted using a functional form suggested by Eq. (1). All the functional forms provided good fits. Note that the two forms showed an onset voltage at approximately −180 V, which is supported by the data. The coefficients obtained from the fits suggested by the model could not be interpreted physically. Yet, if these coefficients were scaled with respect to work function or ion flux, they predicted the arcing activity very well.

Thus, two different methods may be used to predict the arcing activity for a given solar cell. If experimental data are available for that cell at a different ion flux or with a different interconnector, the coefficients of the fitted data may be scaled to predict the arc rates. The second method is to use the semianalytical code. The code can predict the arc rates for any conventional cell under varying environmental conditions. The code predicts the arc rates at the lower voltages accurately. However, it seems to underpredict the arc rates at the high voltages for some of the cells.

References

[1]Thiemann, H., and Bogus, K., "Anomalous Current Collection and Arcing of Solar-Cell Modules in a Simulated High-Density Low-Earth-Orbit Plasma," *ESA Journal*, Vol. 10, No. 1, 1986, pp. 43–57.

[2]Thieman, H., Schunk, R. W., and Bogus, K., "Where Do Negatively Biased Solar Arrays Arc?" *Journal of Spacecraft and Rockets*, Vol. 27, No. 5, 1990, pp. 563–565.

[3]Turner, G. F., and Debrock, S. C., "Large Solar Array Design" *Space Power*, Vol. 8, Nos. 1–2, 1989, pp. 11–22.

[4]Herron, B. G., Bayless, J. R., and Worden, J. D., "High Voltage Solar Array Technology," *Journal of Spacecraft and Rockets*, Vol. 10, No. 4, 1973, pp. 457–462.

[5]Ferguson, D. C., "The Voltage Threshold for Arcing for Solar Cells in LEO-Flight and Ground Test Results," NASA TM-87259, May 1986.

[6]Cho, M., and Hastings, D. E., "Dielectric Charging Processes and Arcing Rates of High Voltage Solar Arrays," *Journal of Spacecraft and Rockets*, Vol. 28, No. 5, 1991, pp. 698–706.

[7]Hastings, D. E., Cho, M., and Kuninaka, H., "The Arcing Rate for a High Voltage Solar Array: Theory, Experiments and Predictions," *Journal of Spacecraft and Rockets*, Vol. 29, No. 4, 1992, pp. 538–554.

[8]Cho, M., and Hastings, D. E., "Computer Particle Simulation of High Voltage Solar Array Arcing Onset," *Journal of Spacecraft and Rockets*, Vol. 30, No. 2, 1993, pp. 189–201.

[9]Hillard, G. B., and Ferguson, D. C., "The SAMPIE Flight Experiment Final Technical Requirements Document," NASA TM-106224, July 1993.

[10]Hillard, G. B., and Ferguson, D. C., "Solar Array Module Plasma Interaction Experiment (SAMPIE): Science and Technology Objectives. " *Journal of Spacecraft and Rockets*, Vol. 30, 1993, pp. 488–494.

[11]Fomenko, V. S., *Handbook of Thermoionic Properties*, Plenum, New York, 1966.

[12]Lide, D. R. (ed.), *CRC Handbook of Chemistry and Physics*, CRC Press, Boca Raton, FL, 1994.

[13]Redhead, P. A., Hobson, J. P., and Kornelsen, E. V., *The Physical Basis of Ultra High Vacuum*, Chapman and Hall, London, 1968.

A. L. Vampola
Associate Editor